

1 **The sensitivity of regional sea level changes**
2 **to the depth of Antarctic meltwater fluxes**

3 **Ian Eisenman¹, Aurora Basinski-Ferris², Emma Beer³, and Laure Zanna²**

4 ¹Scripps Institution of Oceanography, University of California San Diego, La Jolla, CA, USA

5 ²Courant Institute of Mathematical Sciences, New York University, New York, NY, USA

6 ³Department of Earth, Environmental and Planetary Sciences, Rice University, Houston, TX, USA

7 **Key Points:**

- 8 • The depth at which Antarctic meltwater enters the ocean influences global sea level
9 rise patterns
- 10 • The sea level rise signal tends to travel more slowly when meltwater fluxes occur
11 at depth
- 12 • This is dictated primarily by the steric response to the depth of the meltwater fluxes

Abstract

Regional patterns of sea level rise are affected by a range of factors including glacial melting, which has occurred in recent decades and is projected to increase in the future, perhaps dramatically. Previous modeling studies have typically included fluxes from melting glacial ice only as a surface forcing of the ocean or as an offline addition to the sea surface height fields produced by climate models. However, observational estimates suggest that the majority of the meltwater from the Antarctic Ice Sheet actually enters the ocean at depth through ice shelf basal melt. Here we use simulations with an ocean general circulation model in an idealized configuration. The results show that the simulated global sea level rise pattern is sensitive to the depth at which Antarctic meltwater enters the ocean. Further analysis suggests that the response is dictated primarily by the steric response to the depth of the meltwater flux.

Plain Language Summary

The time-varying pattern of sea level rise is projected to cause some coastal communities to be impacted more than others during the coming century. This is influenced by the melting of Antarctic ice. Previous modeling studies have injected this meltwater at the ocean surface, despite observational evidence suggesting that it enters the ocean primarily at depth. Here we use simulations with a model in an idealized configuration to investigate how the sea level rise pattern depends on the depth at which Antarctic meltwater enters the ocean. We find that the sea level change signal tends to travel more slowly across the global ocean when the meltwater enters the ocean at depth. These results have implications for projected regional sea level changes in response to the melting of Antarctic ice.

1 Introduction

Sea level rise is expected to be a major consequence of global warming, with costs from coastal flooding estimated to reach 3% of global GDP by 2100 (Jevrejeva et al., 2018). This impact depends crucially on the time-varying spatial pattern of future sea level rise. Sea level varies regionally due to factors including surface forcing, ocean circulation changes, thermal expansion of seawater, and melting of glacial ice.

Observational estimates of sea level changes during recent decades show substantial spatial variations (Supporting Information (SI) Fig. S1a). Future projections are also characterized by large spatial variations (SI Fig. S1b), although there is considerable uncertainty in the regional structure of projected sea level rise during the coming century (e.g., Gregory et al., 2016; Couldrey et al., 2023).

The melting of glacial ice influences global and regional sea level changes due to the volume added to the ocean, the effect of the freshwater flux on the ocean salinity, and the effect of latent heat of melting on the ocean temperature if the ice melts in the ocean (e.g., Church et al., 2013). Variations in the distribution of ice on land also influence regional sea level due to changes in the shape of the gravitational field of the Earth (e.g., Bamber et al., 2009; Mitrovica et al., 2009; Gomez et al., 2010).

The Antarctic Ice Sheet is the largest body of frozen ice on earth and contains enough ice to cause a global sea level rise of 60 m. Observational studies have found that the mass of the Antarctic Ice Sheet has decreased during recent decades (e.g., Rignot et al., 2011; Velicogna & Wahr, 2013; Bamber et al., 2018; Rignot et al., 2019; Smith et al., 2020; Otosaka et al., 2023). This is associated with an increase in freshwater discharge into the ocean, which impacts global and regional sea level. Floating ice shelves around Antarctica have also been losing mass during recent decades (Shepherd et al., 2010; Paolo et al., 2015; Rignot et al., 2019). Model projections suggest that the rate of ice mass loss

61 in Antarctica will increase in the future, perhaps dramatically (e.g., Nick et al., 2013;
62 Joughin et al., 2014; DeConto & Pollard, 2016; Edwards et al., 2019; Seroussi et al., 2020).

63 Freshwater fluxes into the ocean from glacial mass loss are not included in the com-
64 prehensive global climate model (GCM) simulations carried out for the Coupled Model
65 Intercomparison Project Phase 5 (CMIP5) and Phase 6 (CMIP6) (Taylor et al., 2011;
66 Eyring et al., 2016), which are used for the future projections in the IPCC Assessment
67 Reports. These GCMs do not resolve ice sheet changes, instead typically representing
68 ice sheets essentially as land with a thick snow cover and routing any excess snow ac-
69 cumulation back to the ocean. For example, in the CMIP5 model NCAR CCSM4, if snow
70 accumulation reaches 1 m of snow water equivalent then any additional snowfall is added
71 as runoff to the ocean surface net freshwater flux near the coast (Oleson et al., 2010).

72 Future sea level projections in the IPCC AR5 were created from CMIP5 simula-
73 tion output as the sum of two non-interactive components (Church et al., 2013): (i) the
74 ocean dynamic sea level field plus the global-mean sea level rise due to thermal expan-
75 sion of the ocean, which is computed in each GCM, and (ii) the sea level change from
76 ice sheets, smaller glaciers, and terrestrial water, which is calculated using a separate mod-
77 eling framework (note that the GCMs do not simulate changes in ocean volume). The
78 latter is forced by the global-mean temperature from the GCMs, and it accounts for the
79 mass balance of the Antarctic and Greenland Ice Sheets and smaller glaciers, ground-
80 water storage changes, and the regional influence of gravitational and rotational changes.
81 Hence the sea level projection shown in SI Fig. S1, which is equivalent to the projections
82 used in the IPCC AR5, does not include the influence of glacial melt on ocean circula-
83 tion and dynamic sea level changes. A similar approach is used in the IPCC AR6 based
84 on CMIP6 simulation results.

85 Previous climate modeling studies that have explicitly included fluxes from Antarc-
86 tic ice mass loss have typically treated them as part of the surface forcing of the ocean
87 (e.g., Stouffer et al., 2007; Stammer, 2008; Bronselaer et al., 2018; Golledge et al., 2019;
88 Moorman et al., 2020; Park et al., 2023). However, observational evidence suggests that
89 the largest source of ablation in Antarctica is basal melt of ice shelves in contact with
90 the ocean at depth, with a smaller contribution coming from iceberg calving (Rignot et
91 al., 2013; Depoorter et al., 2013). Consistent with this, *in situ* measurements of the wa-
92 ter column near an Antarctic ice shelf show that the meltwater is most concentrated near
93 a depth of 0.5 km below the surface (Kim et al., 2016). Furthermore, *in situ* measure-
94 ments from another study indicate that Antarctic glacial meltwater is often injected into
95 the coastal ocean considerably deeper than the basal melt source due to overturning in-
96 stability of the outflow from the ice shelf cavity (Garabato et al., 2017). Measurements
97 such as these suggest that a substantial fraction of the meltwater fluxes associated with
98 Antarctic ice mass loss should be applied at a depth greater than 0.5 km below the sur-
99 face in model projections of sea level rise, since GCMs used for future projections nor-
100 mally do not simulate ice shelf ablation or cavity flow.

101 The regional sea level response to Antarctic ice melt may be expected to poten-
102 tially depend on the depth of the forcing, because this forcing can trigger a range of depth-
103 dependent baroclinic responses within the ocean. To this end, a study using satellite mea-
104 surements together with an ocean model found considerable spatial structure of sea level
105 changes near Antarctica associated with the vertical structure of temperature and salin-
106 ity variations from the ablation of the ice shelves (Rye et al., 2014). Similarly, an ocean
107 modeling study found that the simulated temperature and salinity along the continen-
108 tal shelf depends on whether Antarctic ice shelf melt fluxes are applied at the surface
109 or at depth (Mathiot et al., 2017).

110 However, although some previous modeling studies have applied subsurface Antarc-
111 tic ice shelf melt fluxes to study the response of the Southern Ocean stratification, sea
112 ice cover, and pattern of sea surface temperature changes (Pauling et al., 2016, 2017; Merino

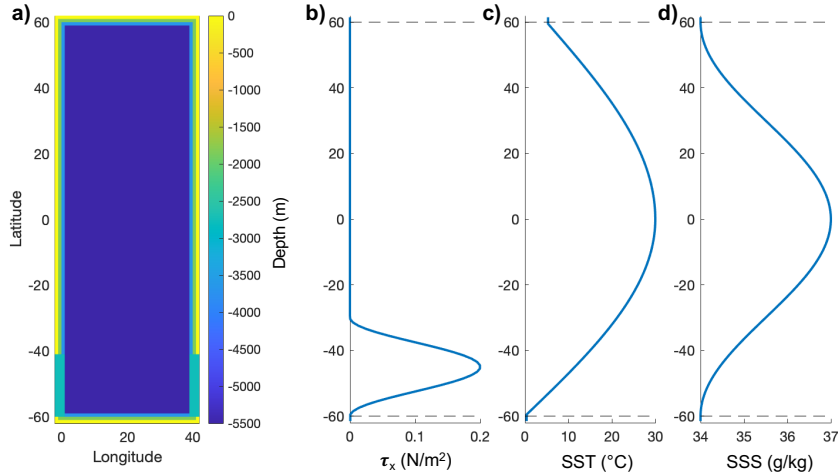


Figure 1. MITgcm simulation setup. (a) Basin bathymetry, including re-entrant Southern Ocean channel. (b) Specified zonal wind stress forcing. (c) Sea surface temperature relaxation field. (d) Sea surface salinity relaxation field. This setup is similar to Munday et al. (2013) but adopts a wider basin and adds continental shelves. During the Spin-up simulation, the temperature and salinity are relaxed to these fields. The relaxation conditions are replaced with specified surface fluxes during the Control and freshwater perturbation simulations following Zika et al. (2018) and Todd et al. (2020).

113 et al., 2018; Mathiot et al., 2017; Jeong et al., 2020; Dong et al., 2022), there has been
 114 a paucity of previous work exploring model simulations of the global sea level response
 115 to subsurface ice melt forcing.

116 Improved understanding of the ocean response to subsurface fluxes from Antarc-
 117 tica can help reduce the uncertainty in the future ocean circulation and climate response
 118 to such perturbations. It may also help elucidate the role of sub-surface processes in trig-
 119 gering ice melt feedbacks that have been proposed in recent studies (Schmidtko et al.,
 120 2014; Bronselaer et al., 2018; Silvano et al., 2018; Golledge et al., 2019; Si et al., 2023).
 121 Here we use ocean GCM simulations in an idealized configuration in order to provide an
 122 initial proof-of-concept to demonstrate how the pattern of sea level rise depends on the
 123 depth of melt fluxes around Antarctica.

124 2 Description of simulations

125 The simulations were carried out with the Massachusetts Institute of Technology
 126 General Circulation Model (MITgcm: Marshall et al., 1997) setup in an idealized rect-
 127 angular ocean basin bathymetry with a re-entrant channel in the Southern Ocean. We
 128 begin with a “Spin-up” simulation, in which we use surface temperature and salinity re-
 129 laxation conditions with relaxation timescales of 10 and 30 days, respectively, as well as
 130 specified surface wind stress over the Southern Ocean. The basin configuration and forc-
 131 ing are shown in Fig. 1. We adopt a relatively coarse horizontal resolution of $1^\circ \times 1^\circ$, us-
 132 ing the Gent-McWilliams (GM) parameterization with an eddy thickness diffusivity of
 133 $1000 \text{ m}^2\text{s}^{-1}$ to represent unresolved mesoscale eddies. We run the model with constant
 134 forcing, rather than including seasonal variations. We use idealized continental shelves
 135 along the basin edges, with the bathymetry decreasing linearly from a depth of 0 m to
 136 the basin depth of 5500 m over 4 degrees, with no-slip boundary conditions along the
 137 walls and bottom of the basin, and we use a channel depth of 2750 m.

138 The simulations are described in more detail in SI Sec. S1. We branch the “Control”, “Surface” freshwater perturbation, and “Deep” freshwater perturbation simulations from the approximately equilibrated state at the beginning of year 7540 of the Spin-up simulation (note that the simulations start at the beginning of year 0). These simulations have the temperature and salinity relaxation condition replaced by specified temperature and salinity fluxes, using a repeating 60-year cycle of daily fluxes that we save from years 7540-7599 of the Spin-up simulation. This follows the method of Zika et al. (2018) and Todd et al. (2020), allowing us to directly examine the response of the ocean to perturbations without damping by the atmosphere. The Control simulation has no freshwater perturbation and hence is similar to the Spin-up simulation, except that it has fixed surface fluxes rather than relaxation conditions. The Surface and Deep simulations have freshwater perturbations as described below. We run each of these three fixed-flux simulations for 240 years while also continuing the Spin-up simulation for 435 years to the end of year 7974.

152 Some previous studies of the ocean response to Antarctic ice melt have applied a horizontal structure of the meltwater flux that is uniform around the Antarctic coast (e.g., Bronselaer et al., 2018), others have scaled the observed pattern (e.g., Snow et al., 2016), and others have used more sophisticated representations such as scaling the linear trend of recent observed ice shelf thickness changes (Moorman et al., 2020). Each of these approaches has strengths and weaknesses. Using a horizontally-uniform forcing is simple and hence conducive to building conceptual understanding, but it may miss key features of the horizontal structure of the ice melt forcing. Scaling observed fluxes could be more accurate, but the fluxes from ice shelves with the largest basal melt rates today will not necessarily increase the most in the future. Amplifying observed ice shelf thickness changes may better capture these sensitivities, but the observational record may be too short to separate interannual variability in basal melt from secular trends, and ice shelf thickness changes do not directly map to basal melt changes due to factors including changes in ice flow across the grounding line (e.g., Adusumilli et al., 2020).

166 In the present study, we apply meltwater fluxes in zonally-uniform bands along the southern border of the basin (60°S), with the aim of providing a first step toward understanding how the sea level adjustment depends on the depth of the flux. The Surface simulation has a 0.1 Sv freshwater flux applied at the surface, and the Deep simulation has a 0.1 Sv freshwater flux applied at a depth of 1 km. The fluxes are held constant throughout the simulations. We do not include cooling from the latent heat of ice shelf melting. This 0.1 Sv flux is similar to the Antarctic Ice Sheet meltwater discharge rates in some projections. Edwards et al. (2019) report an 83 cm Antarctic contribution to sea level during 2000-2100, and DeConto and Pollard (2016) similarly report a 105 cm Antarctic contribution to sea level during 2000-2100, where in both cases we are citing the highest reported scenarios, which use RCP8.5 forcing and include the marine ice cliff instability. These amount to century-averaged freshwater inputs of 0.091 Sv and 0.12 Sv, respectively. The DeConto and Pollard (2016) ice sheet simulation has similarly been used for the forcing in a number of other ocean modeling studies (e.g., Bronselaer et al., 2018; Lago & England, 2019; Schloesser et al., 2019). Note that this imposed 0.1 Sv flux anomaly is about twice as large as the Antarctic Ice Sheet basal melt rate in the current climate, which is estimated by Rignot et al. (2013) to be 1325 gigatons per year, amounting to a freshwater flux of 0.042 Sv. Estimates of future Antarctic meltwater fluxes are subject to uncertainty in the ice sheet model physics, including the hypothesized marine ice cliff instability process, as well as uncertainty in the future radiative forcing scenario. Here we adopt a value on the high side of the uncertainty range in order to emphasize the possible sensitivity to meltwater depth.

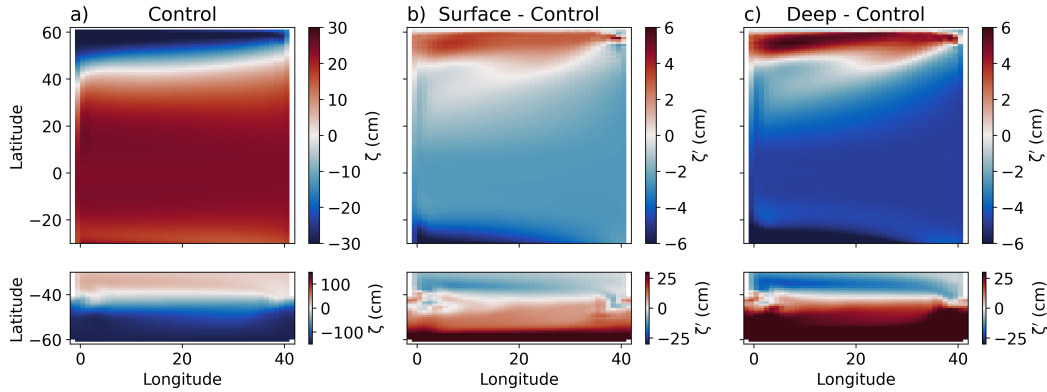


Figure 2. Ocean dynamic sea level ζ . (a) Control simulation. (b) Surface freshwater perturbation simulation anomaly from Control. (c) Deep freshwater perturbation simulation anomaly from Control. The fields are averaged over the last decade of each of the 240-year simulations.

3 Results

We focus on the ocean dynamic sea level ζ , which is the regional pattern of sea surface height; it is defined as the departure from the geoid, with a global-mean value of zero. This is equivalent to the MITgcm output variable “Eta” with the global-mean value removed. Note that ζ is reported in CMIP5 and CMIP6 as the simulation output variable “zos”.

The dynamic sea level ζ in the Control simulation is shown in Fig. 2a. It is positive at latitudes equatorward of about 40°N and 40°S and negative at higher latitudes, which qualitatively resembles the observed global ocean (e.g., Mulet et al., 2021, their Fig. 6a).

The dynamic sea level anomalies from the Control simulations, ζ' , are plotted for the Surface and Deep simulations in Fig. 2b,c. The constant freshwater fluxes applied at the southern edge of the basin in both simulations leads to a higher regional sea level in southern high latitudes, and it broadly causes a reduction in the amplitude of the spatial pattern of ζ in the Control simulation. The key difference between the two simulations is that after the first couple decades, ζ' remains lower in the Northern Hemisphere and higher in the Southern Hemisphere in the Deep simulation, indicating that the applied freshwater flux is spreading more slowly across the ocean basin.

This can be seen clearly in line plots of ζ' averaged spatially over each hemisphere (Fig. 3). Averaged over the final 200 years of the simulations, ζ' is 2.9 cm higher in the Southern Hemisphere than in the Northern Hemisphere in the Deep simulation, compared with just 1.8 cm in the Surface simulation. Note that since ζ is defined to have a global-mean value of zero, the value in the Northern Hemisphere is equal and opposite to the value in the Southern Hemisphere.

The results in Figs. 2 and 3 show that the global sea level change pattern depends critically on the depth of the Antarctic meltwater perturbation, with far field sea level differences that persist throughout the simulations. Broadly, the elevated regional sea level moves more slowly out of the Southern Hemisphere when the freshwater is injected at depth.

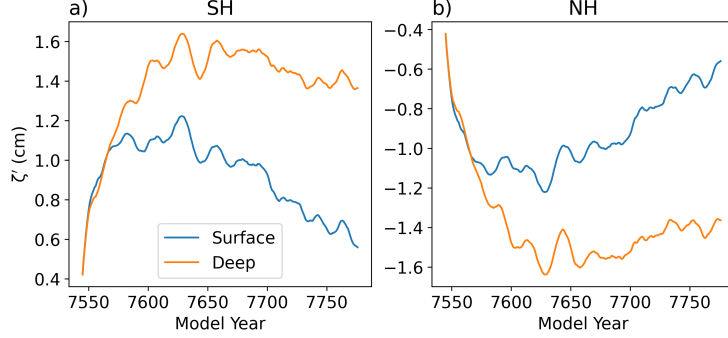


Figure 3. Time series of dynamic sea level anomaly from the Control simulation, ζ' , in the Surface and Deep simulations. (a) Southern Hemisphere spatial mean. (b) Northern Hemisphere spatial mean. All curves are smoothed with a 10-year running mean.

217 4 Sea level change decomposition

218 The dynamic sea level pattern in each perturbed simulation (Surface or Deep) can
 219 be decomposed as follows (e.g., Gill & Niiler, 1973; Yin et al., 2010; Griffies et al., 2014;
 220 Gregory et al., 2019):

$$\zeta' = \underbrace{\frac{p'_b}{\rho_0 g}}_{\text{Mass}} - \underbrace{\frac{1}{\rho_0} \int_{-H}^{\zeta-B} \rho' dz}_{\text{Steric}}, \quad (1)$$

221 where ρ is the ocean density field, ρ_0 is the ocean reference density, g is the acceleration
 222 of gravity, p_b is the ocean bottom hydrostatic pressure, H is the ocean depth, and B rep-
 223 represents the inverse barometer correction due to variations in sea level pressure (adopting
 224 the terminology of Gregory et al., 2019). Here primed quantities represent the anomaly
 225 in a perturbed simulation relative to the Control simulation, with the global mean re-
 226 moved. Note that Eq. (1) is derived from the hydrostatic balance with the near-surface
 227 density approximated to be ρ_0 (e.g., Yin et al., 2010, their Sec. 2b).

228 The first term on the right-hand side of Eq. (1) captures sea level increases due to
 229 seawater being added to the column, i.e., it represents ocean mass redistribution. The
 230 second term on the right-hand side of Eq. (1) captures sea level increases due to the col-
 231 umn becoming less dense without changing its mass, i.e., it represents the sea level change
 232 from local steric changes in the density field. Note that in Boussinesq models such as MIT-
 233 gcm the steric term is not a true expansion or contraction, but it does influence the sim-
 234 ulated currents.

235 The first term is approximately associated with the barotropic component of the
 236 flow, and the second term is approximately associated with the baroclinic component
 237 of the flow (e.g., Savage et al., 2017). Explicitly decomposing the sea level changes into
 238 components associated with the barotropic and baroclinic components of the flow, fol-
 239 lowing the method of McWilliams et al. (2023), leads to qualitatively similar results (Fig. S4).

240 Freshwater injection causes an increase in mass, which leads to a positive contri-
 241 bution to local sea level from the mass term in Eq. (1). This increase in sea level is miti-
 242 gated by the column becoming less dense due to the reduction in salinity from the fresh-
 243 water injection, which leads to a negative contribution to local sea level from the steric
 244 term in Eq. (1).

245 The terms in Eq. (1) can be readily computed from the MITgcm simulation out-
 246 put. The left-hand side is the difference in the dynamic sea level ζ between the perturbed

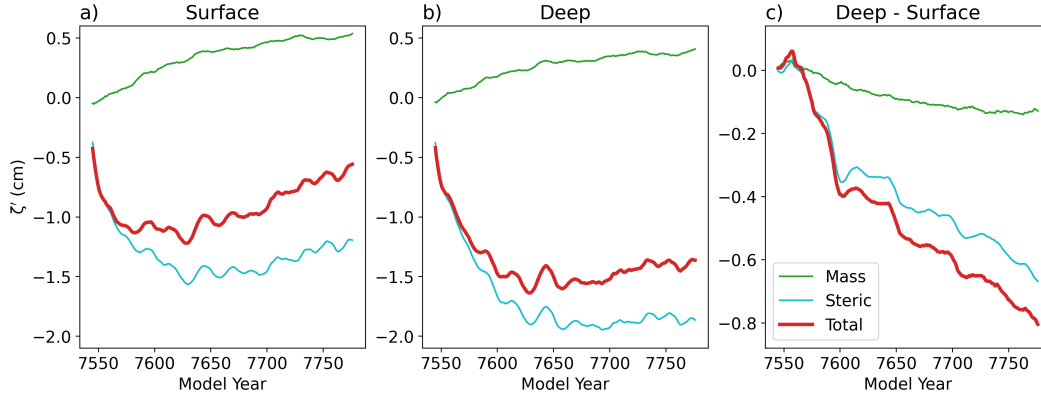


Figure 4. Decomposition of Northern Hemisphere dynamic sea level anomaly ζ' into mass redistribution and steric contributions (Eq. (1)). (a) Surface simulation. (b) Deep simulation. (c) Difference between the two simulations. All curves are smoothed with a 10-year running mean.

247 simulation and the Control simulation. The mass term is computed using the hydrostatic
 248 relationship as the difference between the perturbed simulations in the quantity $\frac{1}{\rho_0} \int_{-H}^{\eta} \rho dz$;
 249 here, the global mean is removed after calculating this term for each simulation. Since
 250 the surface pressure is constant in the MITgcm simulations, we take $B = 0$, and the
 251 steric term is computed as $\frac{1}{\rho_0} \int_{-H}^{\zeta} \rho' dz$, with ρ' defined as above and ζ the dynamic sea
 252 level in the perturbed simulation.

253 The resulting quantities, averaged over the Northern Hemisphere, are plotted in
 254 Fig. 4. Since the dynamic sea level is higher in the hemisphere where freshwater is con-
 255 tinuously injected, ζ' is negative in the Northern Hemisphere in both perturbed simu-
 256 lations (Fig. 3). This is associated primarily with the steric term, which explains most
 257 of the dynamic sea level anomaly ζ' (Fig. 4). The mass term, by contrast, is relatively
 258 small in both perturbed simulations, indicating that this component of the dynamic sea
 259 level spreads rapidly across the globe (Fig. 4), consistent with the rapid propagation of
 260 barotropic waves.

261 As noted above, the difference in ζ' between the two hemispheres is larger in the
 262 Deep simulation, consistent with the injected freshwater flux spreading more slowly across
 263 the basin. The decomposition shows that this difference occurs primarily due to the steric
 264 term (Fig. 4). Although the mass from the injected freshwater spreads quickly into the
 265 Northern Hemisphere in both simulations (near-zero values of green curves in Fig. 4),
 266 the density change from the injected freshwater spreads more slowly (substantial nega-
 267 tive values of blue curves in Fig. 4), especially in the Deep simulation.

268 5 Summary and conclusions

269 Previous climate modeling studies that have explicitly included fluxes from Antarc-
 270 tic ice mass loss have typically treated them as part of the surface forcing of the ocean.
 271 However, observational estimates suggest that the largest source of ablation in Antarc-
 272 tica is basal melt of ice shelves, with the freshwater entering the ocean considerably be-
 273 low the surface. In the present study, we use MITgcm simulations of an idealized ocean
 274 basin with freshwater injected at the surface or at depth in southern high latitudes. The
 275 results suggest that the global sea level change pattern is sensitive to the depth of the
 276 Antarctic meltwater perturbation. When the fluxes are applied at depth the signal tends
 277 to travel more slowly to the Northern Hemisphere. This is consistent with expectations
 278 that the propagation speeds of baroclinic waves will depend on the stratification which

279 is influenced by the depth of the meltwater injection. A decomposition of the sea level
 280 changes shows that the sensitivity to meltwater depth occurs primarily due to differences
 281 in the baroclinic response.

282 Many factors have been neglected in these idealized simulations, including the in-
 283 fluence of realistic basin geometry, the detailed spatial and temporal structure of the melt-
 284 water injection, and the latent heat flux in addition to freshwater injection associated
 285 with ice shelf basal melt. Further research into how these factors would influence the re-
 286 sult is called for. The simulations were carried out with a 1° GCM, raising important
 287 questions about how the results may differ in a higher-resolution model. Furthermore,
 288 the scale of the regional patterns of change in the simulation results (Fig. 2c), while of
 289 a similar order of magnitude to the projected regional pattern of sea level rise during the
 290 coming century (SI Fig. S1), would be considerably smaller than the global-mean sea level
 291 rise due to substantial Antarctic Ice Sheet melting. This is true in general for local pat-
 292 terns of dynamic sea level compared to global mean sea level change. Nonetheless, the
 293 results presented here suggest that sea level changes are sensitive to the depth of fresh-
 294 water injections, which suggests that capturing the depth of Antarctic ice shelf meltwa-
 295 ter may lead to more accurate projections of future regional sea level changes, in par-
 296 ticular when considering local impacts such as increased risk of flooding and storm surge.

297 Open Research Section

298 The MITgcm simulation output and analysis code to generate the figures in this
 299 paper will be posted on FigShare and GitHub by the time of publication. During review
 300 the files are posted at the temporary location

301 http://eisenman.ucsd.edu/code/Eisenman-Basinski-Beer-Zanna-submitted-2024_data-and-code.tgz

302 Acknowledgments

303 This work was supported by National Science Foundation grants OCE-2048590 and OCE-
 304 2048576.

305 References

- 306 Adusumilli, S., Fricker, H. A., Medley, B., Padman, L., & Siegfried, M. R. (2020).
 307 Interannual variations in meltwater input to the Southern Ocean from Antarc-
 308 tic ice shelves. *Nature Geoscience*, 191–194. doi: 10.1038/s41561-020-0616-z
- 309 Bamber, J. L., Riva, R. E. M., Vermeersen, B. L. A., & LeBrocq, A. M. (2009). Re-
 310 assessment of the potential sea-level rise from a collapse of the West Antarctic
 311 Ice Sheet. *Science*, 324(5929), 901–903. doi: 10.1126/science.1169335
- 312 Bamber, J. L., Westaway, R. M., Marzeion, B., & Wouters, B. (2018). The land
 313 ice contribution to sea level during the satellite era. *Environmental Res. Lett.*,
 314 13(9), 063008. doi: 10.1088/1748-9326/aadb2c
- 315 Bronselaer, B., Winton, M., Griffies, S. M., Hurlin, W. J., Rodgers, K. B., Sergienko,
 316 O. V., . . . Russell, J. L. (2018). Change in future climate due to Antarctic
 317 meltwater. *Nature*, 564(7734), 53–58. doi: 10.1038/s41586-018-0712-z
- 318 Church, J., Clark, P., Cazenave, A., Gregory, J., Jevrejeva, S., Levermann, A., . . .
 319 Unnikrishnan, A. (2013). Chapter 13, Sea level change. In T. Stocker et
 320 al. (Eds.), *Climate Change 2013: The Physical Science Basis. Contribution*
 321 *of Working Group I to the Fifth Assessment Report of the Intergovernmental*
 322 *Panel on Climate Change*. Cambridge University Press, Cambridge, UK.
- 323 Couldrey, M. P., Gregory, J. M., Dong, X., Garuba, O., Haak, H., Hu, A. X., . . .
 324 Zanna, L. (2023). Greenhouse-gas forced changes in the Atlantic meridional
 325 overturning circulation and related worldwide sea-level change. *Climate Dy-*
 326 *nam.*, 60(7-8), 2003–2039. doi: 10.1007/s00382-022-06386-y

- 327 DeConto, R. M., & Pollard, D. (2016). Contribution of Antarctica to past and fu-
328 ture sea-level rise. *Nature*, *531*(7596), 591–597. doi: 10.1038/nature17145
- 329 Depoorter, M. A., Bamber, J. L., Griggs, J. A., Lenaerts, J. T. M., Ligtenberg,
330 S. R. M., van den Broeke, M. R., & Moholdt, G. (2013). Calving fluxes and
331 basal melt rates of Antarctic ice shelves. *Nature*, *502*(7469), 89–92. doi:
332 10.1038/nature12567
- 333 Dong, Y., Pauling, A. G., Sadai, S., & Armour, K. C. (2022). Antarctic Ice-
334 Sheet meltwater reduces transient warming and climate sensitivity through
335 the sea-surface temperature pattern effect. *Geophys. Res. Lett.*, *49*(24),
336 e2022GL101249. doi: 10.1029/2022GL101249
- 337 Ducet, N., Traon, P. Y. L., & Reverdin, G. (2000). Global high-resolution map-
338 ping of ocean circulation from TOPEX/Poseidon and ERS-1 and -2. *J. Geo-
339 phys. Res.*, *105*(C8), 19477–19498. ((AVISO Ssalto/Duacs monthly data
340 accessed from <https://www.aviso.altimetry.fr/en/data/data-access.html>)) doi:
341 10.1029/2000JC900063
- 342 Edwards, T. L., Brandon, M. A., Durand, G., Edwards, N. R., Golledge, N. R.,
343 Holden, P. B., . . . Wernecke, A. (2019). Revisiting Antarctic ice loss due
344 to marine ice-cliff instability. *Nature*, *566*(7742), 58–64. doi: 10.1038/
345 s41586-019-0901-4
- 346 Eyring, V., Bony, S., Meehl, G. A., Senior, C. A., Stevens, B., Stouffer, R. J., &
347 Taylor, K. E. (2016). Overview of the Coupled Model Intercomparison Project
348 Phase 6 (CMIP6) experimental design and organization. *Geoscientific Model
349 Development*, *9*(5), 1937–1958. doi: 10.5194/gmd-9-1937-2016
- 350 Garabato, A. C. N., Forryan, A., Dutrieux, P., Brannigan, L., Biddle, L. C., Hey-
351 wood, K. J., . . . Kimura, S. (2017). Vigorous lateral export of the meltwater
352 outflow from beneath an Antarctic ice shelf. *Nature*, *542*(7640), 219–222. doi:
353 10.1038/nature20825
- 354 Gill, A. E., & Niiler, P. P. (1973). Theory of seasonal variability in ocean. *Deep-sea
355 Res.*, *20*(2), 141–177. doi: 10.1016/0011-7471(73)90049-1
- 356 Golledge, N. R., Keller, E. D., Gomez, N., Naughten, K. A., Bernales, J., Trusel,
357 L. D., & Edwards, T. L. (2019). Global environmental consequences
358 of twenty-first-century ice-sheet melt. *Nature*, *566*(7742), 65–72. doi:
359 10.1038/s41586-019-0889-9
- 360 Gomez, N., Mitrovica, J. X., Huybers, P., & Clark, P. U. (2010). Sea level as a sta-
361 bilizing factor for marine-ice-sheet grounding lines. *Nature Geoscience*, *3*(12),
362 850–853. doi: 10.1038/NGEO1012
- 363 Gregory, J., Bouttes, N., Griffies, S. M., Haak, H., Hurlin, W. J., Jungclaus, J., . . .
364 Winton, M. (2016). The Flux-Anomaly-Forced Model Intercomparison Project
365 (FAFMIP) contribution to CMIP6: investigation of sea-level and ocean climate
366 change in response to CO2 forcing. *Geoscientific Model Development*, *9*(11),
367 3993–4017. doi: 10.5194/gmd-9-3993-2016
- 368 Gregory, J., Griffies, S., Hughes, C., Lowe, J., Church, J., Fukimori, I., . . . van de
369 Wal, R. (2019). Concepts and terminology for sea level: Mean, vari-
370 ability and change, both local and global. *Surv. Geophys.*, 1–39. doi:
371 10.1007/s10712-019-09525-z
- 372 Griffies, S. M., Yin, J. J., Durack, P. J., Goddard, P., Bates, S. C., Behrens, E., . . .
373 Zhang, X. B. (2014). An assessment of global and regional sea level for years
374 1993–2007 in a suite of interannual CORE-II simulations. *Ocean Modelling*, *78*,
375 35–89. doi: 10.1016/j.ocemod.2014.03.004
- 376 Jeong, H., Asay-Davis, X. S., Turner, A. K., Comeau, D. S., Price, S. F., Aber-
377 nathey, R. P., . . . Ringler, T. D. (2020). Impacts of Ice-Shelf Melting on
378 Water-Mass Transformation in the Southern Ocean from E3SM simulations. *J.
379 Climate*, *33*(13), 5787–5807. doi: 10.1175/JCLI-D-19-0683.1
- 380 Jevrejeva, S., Jackson, L. P., Grinsted, A., Lincke, D., & Marzeion, B. (2018). Flood
381 damage costs under the sea level rise with warming of 1.5 degrees C and 2

- 382 degrees C. *Environmental Res. Lett.*, *13*(7), 074014. doi: 10.1088/1748-9326/
383 aacc76
- 384 Joughin, I., Smith, B. E., & Medley, B. (2014). Marine ice sheet collapse poten-
385 tially under way for the Thwaites Glacier Basin, West Antarctica. *Science*,
386 *344*(6185), 735–738. doi: 10.1126/science.1249055
- 387 Killworth, P. D. (1996). Time interpolation of forcing fields in ocean models. *J.*
388 *Phys. Oceanogr.*, *26*(1), 136–143. doi: 10.1175/1520-0485(1996)026<0136:
389 TIOFFI>2.0.CO;2
- 390 Kim, I., Hahm, D., Rhee, T. S., Kim, T. W., Kim, C. S., & Lee, S. (2016). The
391 distribution of glacial meltwater in the Amundsen Sea, Antarctica, revealed
392 by dissolved helium and neon. *J. Geophys. Res.*, *121*(3), 1654–1666. doi:
393 10.1002/2015JC011211
- 394 Lago, V., & England, M. H. (2019). Projected slowdown of Antarctic Bottom Wa-
395 ter formation in response to amplified meltwater contributions. *J. Climate*,
396 *32*(19), 6319–6335. doi: 10.1175/JCLI-D-18-0622.1
- 397 Marshall, J., Adcroft, A., Hill, C., Perelman, L., & Heisey, C. (1997). A finite-
398 volume, incompressible Navier Stokes model for studies of the ocean on parallel
399 computers. *J. Geophys. Res.*, *102*(C3), 5753–5766. doi: 10.1029/96JC02775
- 400 Mathiot, P., Jenkins, A., Harris, C., & Madec, G. (2017). Explicit representation
401 and parametrised impacts of under ice shelf seas in the z^* coordinate ocean
402 model NEMO 3.6. *Geoscientific Model Development*, *10*(7), 2849–2874. doi:
403 10.5194/gmd-10-2849-2017
- 404 McWilliams, J. C., Molemaker, J., & Damien, P. (2023). Baroclinic sea-level. *ESS*
405 *Open Archive*. doi: 10.22541/essoar.169272214.48059542/v1
- 406 Merino, N., Jourdain, N. C., Sommer, J. L., Goosse, H., Mathiot, P., & Durand,
407 G. (2018). Impact of increasing Antarctic glacial freshwater release on re-
408 gional sea-ice cover in the Southern Ocean. *Ocean Modelling*, *121*, 76–89. doi:
409 10.1016/j.ocemod.2017.11.009
- 410 Mitrovica, J. X., Gomez, N., & Clark, P. U. (2009). The sea-level fingerprint of
411 West Antarctic collapse. *Science*, *323*(5915), 753–753. doi: 10.1126/science
412 .1166510
- 413 Moorman, R., Morrison, A., & Hogg, A. (2020). Thermal responses to Antarctic
414 Ice Shelf melt in an eddy-rich global ocean-sea ice model. *J. Climate*, *33*(15),
415 6599–6620. doi: 10.1175/JCLI-D-19-0846.1
- 416 Mulet, S., Rio, M.-H., Etienne, H., Artana, C., Cancet, M., Dibarboure, G., ...
417 Strub, P. T. (2021). The new CNES-CLS18 global mean dynamic topography.
418 *Ocean Science*, *17*(3), 789–808. Retrieved from [https://os.copernicus.org/
419 articles/17/789/2021/](https://os.copernicus.org/articles/17/789/2021/) doi: 10.5194/os-17-789-2021
- 420 Munday, D. R., Johnson, H. L., & Marshall, D. P. (2013). Eddy saturation of equili-
421 brated circumpolar currents. *J. Phys. Oceanogr.*, *43*(3), 507–532. doi: 10.1175/
422 JPO-D-12-095.1
- 423 Nick, F. M., Vieli, A., Andersen, M. L., Joughin, I., Payne, A., Edwards, T. L.,
424 ... van de Wal, R. S. W. (2013). Future sea-level rise from Greenland’s
425 main outlet glaciers in a warming climate. *Nature*, *497*(7448), 235–238. doi:
426 10.1038/nature12068
- 427 Oleson, K. W., Lawrence, D. M., Bonan, G. B., Flanner, M. G., Kluzek, E.,
428 Lawrence, P. J., ... Thornton, P. E. (2010). Technical description
429 of version 4.0 of the community land model (clm) [Computer software
430 manual]. National Center for Atmospheric Research, Boulder, CO,
431 http://www.cesm.ucar.edu/models/cesm2/land/CLM50_Tech_Note.pdf.
- 432 Otosaka, I. N., Shepherd, A., Ivins, E. R., Schlegel, N. J., Amory, C., van den
433 Broeke, M. R., ... Wouters, B. (2023). Mass balance of the Greenland and
434 Antarctic ice sheets from 1992 to 2020. *Earth System Sci. Data*, *15*(4), 1597–
435 1616. doi: 10.5194/essd-15-1597-2023
- 436 Paolo, F. S., Fricker, H. A., & Padman, L. (2015). Volume loss from Antarctic ice

- 437 shelves is accelerating. *Science*, *348*(6232), 327–331. doi: 10.1126/science
 438 .aaa0940
- 439 Park, J. Y., Schloesser, F., Timmermann, A., Choudhury, D., Lee, J. Y., &
 440 Nellikattil, A. B. (2023). Future sea-level projections with a coupled
 441 atmosphere-ocean-ice-sheet model. *Nature Comm.*, *14*(1), 636. doi:
 442 10.1038/s41467-023-36051-9
- 443 Pauling, A. G., Bitz, C. M., Smith, I. J., & Langhorne, P. J. (2016). The re-
 444 sponse of the Southern Ocean and Antarctic sea ice to freshwater from
 445 ice shelves in an earth system model. *J. Climate*, *29*(5), 1655–1672. doi:
 446 10.1175/JCLI-D-15-0501.1
- 447 Pauling, A. G., Smith, I. J., Langhorne, P. J., & Bitz, C. M. (2017). Time-
 448 dependent freshwater input from ice shelves: Impacts on Antarctic sea ice and
 449 the Southern Ocean in an earth system model. *Geophys. Res. Lett.*, *44*(20),
 450 10454–10461. doi: 10.1002/2017GL075017
- 451 Rignot, E., Jacobs, S., Mouginot, J., & Scheuchl, B. (2013). Ice-shelf melting around
 452 Antarctica. *Science*, *341*(6143), 266–270. doi: 10.1126/science.1235798
- 453 Rignot, E., Mouginot, J., Scheuchl, B., van den Broeke, M., van Wessem, M. J.,
 454 & Morlighem, M. (2019). Four decades of Antarctic Ice Sheet mass bal-
 455 ance from 1979–2017. *Proc. Natl. Acad. Sci. U.S.A.*, *116*(4), 1095–1103. doi:
 456 10.1073/pnas.1812883116
- 457 Rignot, E., Velicogna, I., van den Broeke, M. R., Monaghan, A., & Lenaerts, J.
 458 (2011). Acceleration of the contribution of the Greenland and Antarc-
 459 tic ice sheets to sea level rise. *Geophys. Res. Lett.*, *38*, L05503. doi:
 460 10.1029/2011GL046583
- 461 Rye, C. D., Garabato, A. C. N., Holland, P. R., Meredith, M. P., Nurser, A. J. G.,
 462 Hughes, C. W., ... Webb, D. J. (2014). Rapid sea-level rise along the Antarc-
 463 tic margins in response to increased glacial discharge. *Nature Geoscience*,
 464 *7*(10), 732–735. doi: 10.1038/NNGEO2230
- 465 Savage, A. C., Arbic, B. K., Richman, J. G., Shriver, J. F., Alford, M. H., Buijs-
 466 man, M. C., ... Zamudio, L. (2017). Frequency content of sea surface height
 467 variability from internal gravity waves to mesoscale eddies. *Journal of Geo-*
 468 *physical Research: Oceans*, *122*(3), 2519–2538. Retrieved from [https://](https://agupubs.onlinelibrary.wiley.com/doi/abs/10.1002/2016JC012331)
 469 [agupubs.onlinelibrary.wiley.com/doi/abs/10.1002/2016JC012331](https://doi.org/10.1002/2016JC012331) doi:
 470 <https://doi.org/10.1002/2016JC012331>
- 471 Schloesser, F., Friedrich, T., Timmermann, A., DeConto, R. M., & Pollard, D.
 472 (2019). Antarctic iceberg impacts on future Southern Hemisphere climate.
 473 *Nature Climate Change*, *9*(9), 672–677. doi: 10.1038/s41558-019-0546-1
- 474 Schmidtko, S., Heywood, K. J., Thompson, A. F., & Aoki, S. (2014). Multidecadal
 475 warming of Antarctic waters. *Science*, *346*(6214), 1227–1231. doi: 10.1126/
 476 science.1256117
- 477 Seroussi, H., Nowicki, S., Payne, A. J., Goelzer, H., Lipscomb, W. H., Abe Ouchi,
 478 A., ... Zwinger, T. (2020). ISMIP6 Antarctica: a multi-model ensemble
 479 of the Antarctic ice sheet evolution over the 21st century. *The Cryosphere*
 480 *Discussions*, *2020*, 1–54. doi: 10.5194/tc-2019-324
- 481 Shepherd, A., Wingham, D., Wallis, D., Giles, K., Laxon, S., & Sundal, A. V.
 482 (2010). Recent loss of floating ice and the consequent sea level contribution.
 483 *Geophys. Res. Lett.*, *37*, L13503. doi: 10.1029/2010GL042496
- 484 Si, Y. D. F., Stewart, A. L., & Eisenman, I. (2023). Heat transport across the
 485 Antarctic Slope Front controlled by cross-slope salinity gradients. *Sci. Adv.*,
 486 *9*(18), eadd7049. doi: 10.1126/sciadv.add7049
- 487 Silvano, A., Rintoul, S. R., Pena-Molino, B., Hobbs, W. R., van Wijk, E., Aoki, S.,
 488 ... Williams, G. D. (2018). Freshening by glacial meltwater enhances melt-
 489 ing of ice shelves and reduces formation of Antarctic Bottom Water. *Science*
 490 *Advances*, *4*(4), eaap9467. doi: 10.1126/sciadv.aap9467
- 491 Smith, B., Fricker, H. A., Gardner, A. S., Medley, B., Nilsson, J., Paolo, F. S.,

- 492 ... Zwally, H. J. (2020). Pervasive ice sheet mass loss reflects compet-
 493 ing ocean and atmosphere processes. *Science*, *368*(6496), 1239–1242. doi:
 494 10.1126/science.aaz5845
- 495 Snow, K., Hogg, A. M., Sloyan, B. M., & Downes, S. M. (2016). Sensitivity of
 496 Antarctic Bottom Water to Changes in Surface Buoyancy fluxes. *J. Climate*,
 497 *29*(1), 313–330. doi: 10.1175/JCLI-D-15-0467.1
- 498 Stammer, D. (2008). Response of the global ocean to Greenland and Antarctic ice
 499 melting. *J. Geophys. Res.*, *113*(C6), C06022. doi: 10.1029/2006JC004079
- 500 Stouffer, R. J., Seidov, D., & Haupt, B. J. (2007). Climate response to external
 501 sources of freshwater: North Atlantic versus the Southern Ocean. *J. Climate*,
 502 *20*(3), 436–448. doi: 10.1175/JCLI4015.1
- 503 Taylor, K. E., Stouffer, R. J., & Meehl, G. A. (2011). An overview of CMIP5 and
 504 the experiment design. *Bull. Amer. Meteor. Soc.*, *93*(4), 485–498. doi: 10
 505 .1175/BAMS-D-11-00094.1
- 506 Todd, A., Zanna, L., Couldrey, M., Gregory, J., Wu, Q., Church, J. A., ... Zhang,
 507 X. (2020). Ocean-only FAFMIP: Understanding regional patterns of ocean
 508 heat content and dynamic sea level change. *J. Adv. In Modeling Earth Sys-*
 509 *tems*, *12*, e2019MS002027. doi: 10.1029/2019MS002027
- 510 Velicogna, I., & Wahr, J. (2013). Time-variable gravity observations of ice sheet
 511 mass balance: Precision and limitations of the GRACE satellite data. *Geophys.*
 512 *Res. Lett.*, *40*(12), 3055–3063. doi: 10.1002/grl.50527
- 513 Yin, J. J., Griffies, S. M., & Stouffer, R. J. (2010). Spatial variability of sea level
 514 rise in twenty-first century projections. *J. Climate*, *23*(17), 4585–4607. doi: 10
 515 .1175/2010JCLI3533.1
- 516 Zika, J. D., Skliris, N., Blaker, A. T., Marsh, R., Nurser, A. J. G., & Josey, S. A.
 517 (2018). Improved estimates of water cycle change from ocean salinity: the
 518 key role of ocean warming. *Environmental Res. Lett.*, *13*(7), 074036. doi:
 519 10.1088/1748-9326/aace42

Supporting Information

520

S1 Description of simulation

521

522 We initially run the model for 300 years. We then test the sensitivity of model pa-
523 rameters that control mixing, diffusion, and convection, and we adjust the parameters
524 in order to simulate a relatively realistic ocean circulation including the global residual
525 meridional overturning circulation. Specifically, we change the parameter “diffKrT/S”,
526 which is the background vertical diffusivity and was set by default during the sensitiv-
527 ity testing to vary with depth between $0.1 \times 10^{-4} \text{ m}^2\text{s}^{-2}$ and $1.5 \times 10^{-4} \text{ m}^2\text{s}^{-2}$, to instead
528 vary with depth between $0.5 \times 10^{-4} \text{ m}^2\text{s}^{-2}$ and $1.75 \times 10^{-4} \text{ m}^2\text{s}^{-2}$ in the Spin-up simu-
529 lation.

530 We then run the Spin-up simulation until the end of year 7974. We find that the
531 global volume-mean temperature and salinity evolve approximately exponentially toward
532 their equilibrium values with e-folding timescales of 1090 years and 1340 years, respec-
533 tively, after the first few thousand years (Fig. S2).

534 The Control, Surface, and Deep simulations are branched from the beginning of
535 year 7540 of the Spin-up simulation. We set the Spin-up simulation to save daily out-
536 put of the temperature and salinity relaxation fields during years 7540–7599, which we
537 use to generate a 60-year cycle of daily fluxes. Note that the simulations with specified
538 fluxes use the “Qnet” and “saltflux” surface forcing options in MITgcm. This requires
539 changing the sign of the Spin-up simulation output to be used as input in the simula-
540 tions with specified fluxes. In order to preserve the daily-mean values when the model
541 linearly interpolates between values at the midpoint of each day, we use a process called
542 “diddling” to adjust the daily data (Killworth, 1996). The perturbations in the Surface
543 and Deep simulations are added as water at 0 psu and 0°C using the “AddMass” option
544 in MITgcm.

545 We select year 7540 as the start time of the simulations with specified fluxes be-
546 cause (i) it allows the Spin-up simulation to reach a relatively high level of equilibration
547 (SI Fig. S2) and (ii) the 60-year mean during years 7540–7599 of the global-means of both
548 flux fields is approximately zero (SI Fig. S3). The latter condition is important because
549 the global volume-mean temperature and salinity in the Control simulation evolves at
550 a constant rate that is set by the global-mean values of these fixed surface fluxes. The
551 drift in volume-mean temperature and salinity in the Control simulation is $2.5 \times 10^{-5} \text{ K/yr}$
552 and $7 \times 10^{-6} \text{ g/kg/yr}$, which is considerably smaller than some other studies that used
553 a similar method (e.g., 0.02 K/yr and 0.02 g/kg/yr in Zika et al., 2018).

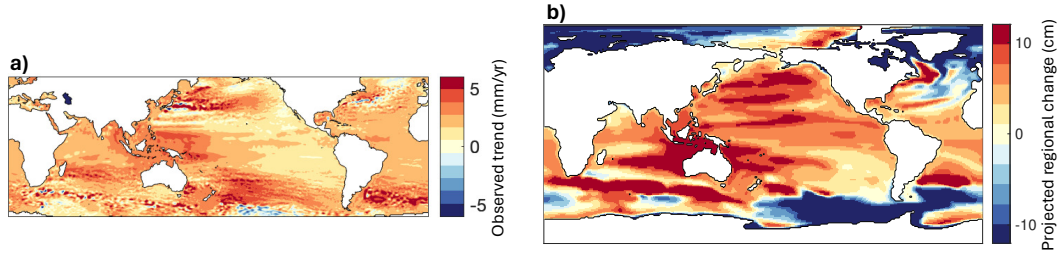


Figure S1. Maps of observed and projected regional sea level changes. (a) Observed sea level trends during 1993 to 2018, computed using the AVISO satellite altimetry dataset (Ducret et al., 2000). Only the latitude range 60°S–60°N is plotted due to limited data coverage in higher latitudes. (b) Projected future regional pattern of sea level change generated using the GFDL-ESM2M simulation of the CMIP5 scenario RCP 4.5, shown as the average during years 2090-2099 compared with 2006-2015. The simulation results include dynamic contributions due to changes in ocean density and mass redistribution, as well as land ice and terrestrial water components which are calculated using a separate modeling framework (for details see main text as well as Church et al., 2013). Here the global-mean sea level rise, which is 41 cm, is subtracted from the future projection in order to better illustrate the regional patterns.

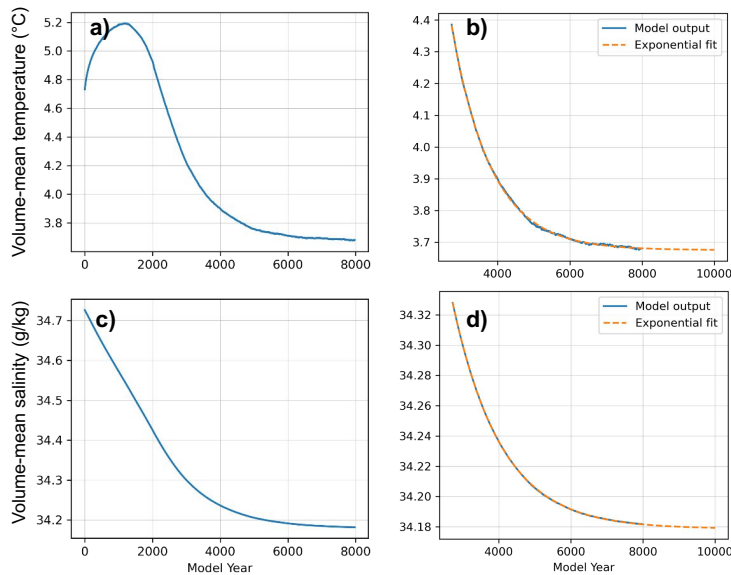


Figure S2. Evolution of (a,b) temperature and (c,d) salinity during (a,c) the entire Spin-up simulation and (b,d) the final 5000 years of the 7975-year Spin-up simulation. The dashed lines show exponential fits, with e-folding timescales of 1090 years for temperature and 1340 years for salinity.

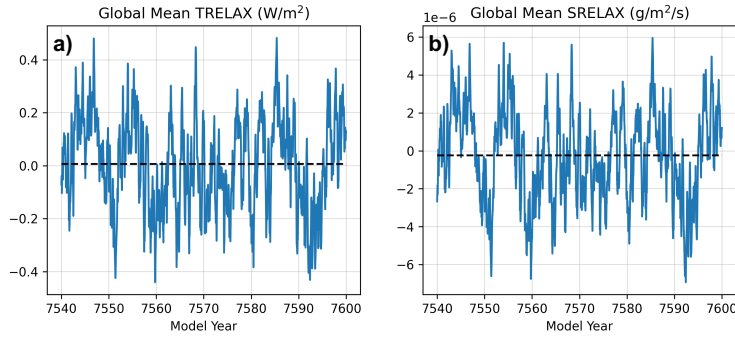


Figure S3. Evolution of the global-mean value of (a) the temperature flux and (b) the salinity flux due to the surface relaxation conditions during years 7540-7599 of the Spin-up simulation. The black dashed line shows the time average. The fluxes during the time period plotted here are used as the fixed surface fluxes in the Control, Surface, and Deep simulations.

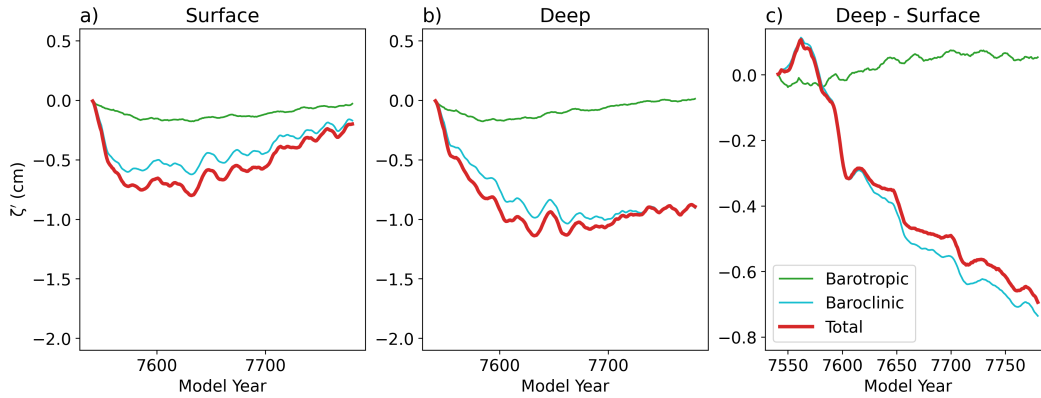


Figure S4. As in Fig. 4, but using a decomposition of Northern Hemisphere dynamic sea level anomaly ζ' into components associated with barotropic and baroclinic circulation changes (McWilliams et al., 2023), rather than components associated with mass redistribution and steric changes (Gill & Niiler, 1973; Yin et al., 2010; Griffies et al., 2014; Gregory et al., 2019). Here, only the sea level away from the continental shelves is decomposed, as per the requirements in McWilliams et al. (2023).